Atom ordering in the tetrahedral framework of zeolite A

1993 J. Phys.: Condens. Matter 5 4125

(http://iopscience.iop.org/0953-8984/5/25/003)

J. Phys.: Condens. Matter 5 (1993) 4125–4136. Printed in the UK

Atom ordering in the tetrahedral framework of zeolite A

Carlos P Herrero

Instituto de Ciencia de Materiales, CSIC Serrano, 115 duplicado, 28006 Madrid, Spain

Received 11 December 1992, in final form 15 March 1993

Abstract. The short-range and long-range order of the distribution of Si and Al atoms in the tetrahedral framework of zeolite A is analysed by the Monte Carlo (MC) method, in a composition range from 0.25 to 0.5 Al mole fraction. An interatomic potential model previously applied to aluminosilicates, including long-range Coulomb and atomic polarization energies, is employed. The short-range site correlations found from the MC simulations are in good agreement with those derived from earlier nuclear magnetic resonance data. In particular, we find that Al atoms in neighbouring tetrahedra are avoided. Long-range ordering with Al and Si atoms alternating in the network is found for Al fractions higher than 0.44. The resulting atom ordering is compared with that obtained by using an Ising-like model, in which only nearest-neighbour interactions between tetrahedral atoms are included. The effect of the non-ergodicity of the MC simulations for compositions showing sub-lattice ordering is discussed and related to a change of space group of the material (from $Pm\bar{3}m$ for low Al content to $Fm\bar{3}c$ for Al atomic fraction near 0.5).

1. Introduction

Zeolites form an important class of aluminosilicate materials with framework structure made up of corner-linked AlO_4 and SiO_4 tetrahedra. Many different geometries are known, and the synthesis of new zeolitic structures continues to be at present a challenge for chemists. In the last thirty years, several industrially important zeolites having no natural counterparts have been synthesized. Prominent among these synthetic materials is the so-called A-type zeolite, which since its discovery has been the subject of numerous studies, and is well known for its industrial applications as sorbent and molecular sieve [1].

Several theoretical works have been carried out in order to investigate the stability of the ions and molecules bound to the zeolite-A framework. Most of these works were based on classical potential energy functions [2] and molecular orbital methods [3], and were focused on the analysis of the interactions between the framework and the adsorbed species. In recent years, molecular dynamics simulations have been performed to study the structural and dynamical properties of the adsorbed ions as well as those of the framework itself [4–6].

One of the most outstanding structural aspects affecting the physico-chemical properties of zeolites in general is the distribution of Si and Al atoms over the tetrahedral sites of the framework. For zeolite A with equal mole fractions of Si and Al, it is now accepted that these atoms alternate in the network in a well-defined long-range pattern [7, 8]. The picture is not so clear for lower Al content, where currently the only generally accepted feature of the atom distribution is the avoidance of Al atoms in nearest tetrahedra, a characteristic of hydrothermally synthesized zeolites [9, 10]. Deep insight into the Si, Al distribution in the framework of zeolite A has been obtained by means of ^{29}Si magic-angle-spinning nuclear magnetic resonance (NMR) spectroscopy, which allows us to quantify the concentrations of the different environments of the Si atoms present in the material [11, 12]. Other

0953-8984/93/254125+12$07.50

experimental techniques, such as Raman spectroscopy, can be used to study the arrangement of the Si and Al atoms, although the interpretation of the results is not so direct as in the case of ^{29}Si NMR [13].

Monte Carlo (MC) simulations have been employed to study different structural problems related to substitutional disorder in aluminosilicates [14–17]. This computational technique allows us to study the atom ordering over a given framework once an interatomic potential model is chosen. An advantage of MC simulations over energy minimization is the fact that the former are carried out at finite temperatures ($T > 0$), and thus take into account thermal effects, which have been reported to be non-negligible at the formation temperature of these materials [18].

In this paper, the Si, Al distribution in A-type zeolites is studied by a MC method. Two potential models are considered: in model A, we assume only Al–O–Al avoidance, while model B includes long-range interactions between the atoms. The simulation results are used to study the short- and long-range order of the atom distribution.

2. Model and methods

The framework of zeolite A is composed of sodalite cages (truncated octahedra) linked through double tetramer rings to form a three-dimensional system of channels with eight-membered ring windows. A sketch of this network is shown in figure 1, where filled and open circles represent tetrahedral (T) sites corresponding to two sub-lattices T_a and T_b, which will be employed in the discussion below. O atoms, located approximately half-way between tetrahedral atoms, are omitted for simplicity of the figure.

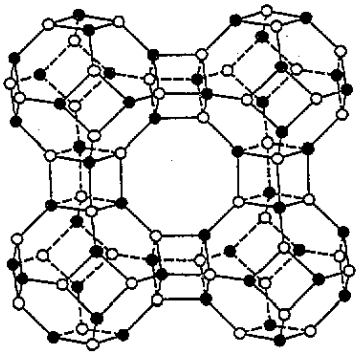

Figure 1. Sketch of the zeolite-A framework showing two different subsets (filled and open circles) of tetrahedral sites, employed in the discussion of the atom ordering. O atoms, located approximately half-way between tetrahedral atoms, are omitted for simplicity. The diameter of the eight-membered ring, measured as the distance between T atoms across the ring, is about 8 Å.

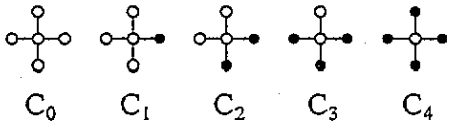

Figure 2. Sketch of the different environments of the Si atoms in the zeolite-A framework. Each circle represents a tetrahedral atom (open circles, Si; filled circles, Al). O atoms located between the T atoms are not displayed. C_n denote the concentrations of the different groups of T atoms, which are proportional to the ^{29}Si NMR line intensities.

We have considered a cubic simulation cell with side length $a = 24.555$ Å, generated as a $2\times2\times2$ supercell of the structure given by Pluth and Smith [19] with space group $Pm\bar{3}m$. The framework geometry is assumed to be fixed, independently of the Al content and the

T-atom distribution. The net negative charge of the framework, caused by the presence of Al atoms, is compensated by exchangeable Na^+ cations, located in the channels. Thus the composition of our simulation cell is $Na_n(Al_nSi_{192-n}O_{384})$, with n in the range 48–96. x_{Al} and x_{Si} will denote the mole fractions of Al and Si, respectively, which are given by $x_{Al} = n/192$ and $x_{Si} = 1 - x_{Al}$. In the following, the expression T–O–T (T: tetrahedral atom, Si or Al) is simplified to T–T.

Given the experimental evidence for the avoidance of Al atoms in adjacent tetrahedra, the potential model *A* was chosen as an effective repulsive interaction, J_{Al-Al}, between Al atoms in nearest T sites. We have taken $J_{Al-Al} = 10k_BT_F$ (k_B, Boltzmann constant; T_F, formation temperature of A-type zeolites, $T_F \simeq 400$ K), that corresponds to an effective energy of about 33 kJ mol^{-1} and is very close to the values found experimentally for the endothermic process 2 Al–O–Si → Al–O–Al + Si–O–Si in aluminosilicate structures [20].

In the potential model B, the lattice energy is calculated as a sum of three contributions: short-range dispersion–repulsion energy, Coulomb interaction and O polarization. The Coulomb energy is obtained by Ewald summation, assuming point charges on the atomic sites. A relevant parameter for the calculation of this energy is the net charge difference between Si and Al atoms in the framework ($\delta = q_{Si} - q_{Al}$). This difference is at present not well known, and we have used the value $\delta = 0.26$ (in units of the elementary charge), which has been previously found to give the best agreement between the Si-environment concentrations derived from ^{29}Si NMR spectra of A-type zeolites and those obtained from MC simulations [21]. This value of δ is clearly lower than that corresponding to a pure ionic model ($\delta = 1$), which predicts an atom distribution in apparent disagreement with the NMR results. In fact, the formal charge difference $\delta = 1$ gives for low Al content an Si, Al distribution more ordered than that found experimentally [21]. The O polarization energy is calculated as

$$U^P = -\tfrac{1}{2}\alpha_0 \sum_{k=1}^{2N_T} |E_k|^2 \tag{1}$$

where α_0 is the O polarizability ($\alpha_0 = 1.984$ Å^3) [22], E_k is the electric field at O k, and the sum is extended to the $2N_T$ O atoms in the simulation cell (N_T is the number of T atoms in the cell).

The short-range dispersion–repulsion energy is approximated by a Buckingham potential, in which the interaction between atoms i and j is described by

$$V(r_{ij}) = A_{ij} \exp(-r_{ij}/\rho_{ij}) - C_{ij}/r_{ij}^6 \tag{2}$$

and the parameters A_{ij}, ρ_{ij}, and C_{ij} were taken from Ooms *et al* [22]. This kind of interatomic potential has been found to be adequate to model structural aspects of aluminosilicate lattices [23], and in particular those of the zeolite-A framework [24]. For a given composition and for a fixed lattice geometry, this short-range potential gives a constant contribution to the lattice energy, independent of the T-atom distribution (the numbers of Al–O and Si–O bonds are constant). More details on the energy calculations with this potential model are given elsewhere [25].

We have simulated the Si, Al distribution for 25 framework compositions in the range $n = 48$–96 ($x_{Al} = 0.25$–0.5). For each composition, the canonical ensemble (NVT) was sampled by the Metropolis procedure [26, 27] at temperature $T_F = 400$ K. The sampling consists of 5×10^5 MC steps, each one including an attempt to interchange each Al atom in the simulation cell with a nearby Si atom. To equilibrate the system at the temperature T_F, a

'simulated annealing' process was carried out prior to each run. Such a method consists in beginning a simulation at a high temperature ($T \simeq 2000$ K in our case) and then decreasing slowly T down to T_F. This procedure reduces the risk that the simulation at T_F begins at a metastable microstate (atom configuration), far from thermodynamic equilibrium [28].

In order to analyse the ordering of the tetrahedral atoms, we associate a variable σ_i with each T site i, where $\sigma_i = 1$ or -1 respectively according to whether the site is occupied by an Al or an Si atom. We characterize the short-range order of the atom distribution by the two-site correlations:

$$S_1 = \langle \sigma_i \sigma_j \rangle_{nn} \tag{3}$$

$$S_2 = \langle \sigma_i \sigma_j \rangle_{sn} \tag{4}$$

where nn indicates that S_1 is obtained by averaging over nearest-neighbour T sites, and sn means second-neighbour sites. As explained below, these pair correlations are related with the intensities of the components appearing in the ^{29}Si NMR spectra of zeolites. These spectra consist of up to five Si(nAl) signals, where n (which can be 0, 1, 2, 3 or 4) denotes the number of Al atoms linked, via O bridges, to an Si atom [11, 12]. The corresponding line intensities are proportional to the concentrations C_n of the different Si environments shown in figure 2.

The zeolite-A framework is loose packed in the sense that one can define two sub-lattices of tetrahedral sites (say T_a and T_b) in such a way that the four nearest neighbours of a T_a site are T_b sites and vice versa (see figure 1). X-ray diffraction analyses indicated that for $x_{Al} = 0.5$, Al and Si alternate in the network, occupying respectively sites T_a and T_b in a well defined long-range order pattern [19, 8]. The presence of long-range ordering in the atom distribution can be studied from our MC simulations by calculating the average atom occupancy of both sub-lattices. With this purpose, we define an order parameter L by

$$x_{Al,a} = x_{Al}(1 + L) \tag{5}$$

where $x_{Al,a}$ denotes the mole fraction of Al atoms on sub-lattice T_a. With similar definitions for $x_{Al,b}$, $x_{Si,a}$ and $x_{Si,b}$, one has

$$x_{Si,a} = 1 - x_{Al,a} = x_{Si} - x_{Al}L \tag{6}$$

$$x_{Al,b} = x_{Al}(1 - L) \tag{7}$$

$$x_{Si,b} = 1 - x_{Al,b} = x_{Si} + x_{Al}L. \tag{8}$$

L takes its extreme values (1 and -1) when all Al atoms are located on the same sub-lattice (T_a or T_b), and equals zero when both sub-lattices are equally occupied. In the unit cell with space group $Pm\bar{3}m$ employed in the generation of our simulation cell, all T sites are crystallographically equivalent. In the course of the MC simulations, the Si and Al atoms are free to distribute over the tetrahedral sites of the framework, according to the selected interatomic potential, without any symmetry constraint. The symmetry breaking (different T_a and T_b sites; space group $Fm\bar{3}c$ [19]) appears naturally in the course of the simulations for x_{Al}/x_{Si} near 1, when the average atom occupancies of each type of T site are different (see below).

3. Results

The results of the simulations carried out with both interaction potentials *A* and *B* are in agreement with the avoidance of Al atoms in nearest tetrahedra (the so-called Loewenstein rule in mineralogy [29]). If this pair avoidance is strictly fulfilled, the two-site correlation S_1 is a linear function of the Al content ($S_1 = 1-4x_{Al}$), as shown in figure 3 (broken line). As a reference, we present also the x_{Al} dependence of S_1 for a random atom distribution, which is given by $S_1^R = 1-4x_{Al}x_{Si}$ (dotted line). The filled squares in figure 3 were obtained from our MC simulations for model B, which includes long-range interaction potentials. These points lie close to the line corresponding to the strict avoidance of Al–Al pairs, in agreement with the conclusions of ^{29}Si NMR studies [9, 10]. In the whole range $n = 48-96$, we obtain a number of Al–Al pairs in nearest-neighbour T sites smaller than 5% of that expected for a random T-atom distribution. For model A (only nearest-neighbour interactions), the number of Al–Al pairs is negligible, giving values of the S_1 correlation lying exactly on the broken line of figure 3. We note in passing that in the case $x_{Al} = x_{Si} = 0.5$, this model is mathematically equivalent to an Ising model for an antiferromagnet in zero magnetic field [30].

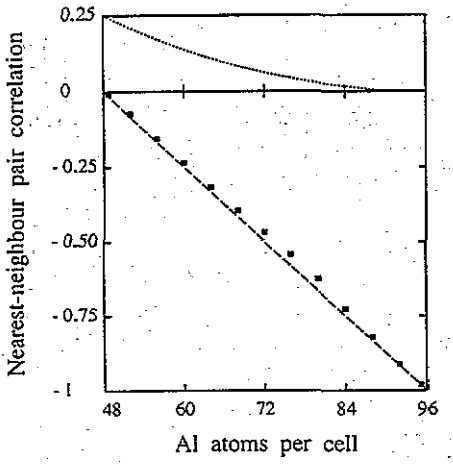

Figure 3. Nearest-neigbour correlation, S_1, versus Al content. The broken curve corresponds to the total avoidance of Al atoms in neighbouring T sites. Filled squares are data points obtained from MC simulations for the interaction model B. The dotted curve corresponds to a random atom arrangement.

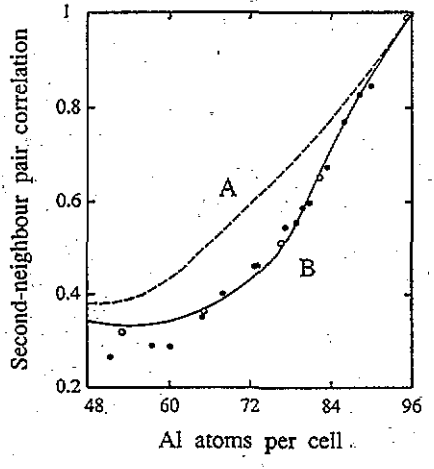

Figure 4. Second-neighbour pair correlation, S_2, versus Al loading obtained from MC simulations for the interaction models A (broken curve) and B (continuous curve). Filled and open circles were obtained by using equation (11) from ^{29}Si NMR spectra obtained by Bennett *et al* [9] and Jarman *et al* [10], respectively.

Assuming that nearest-neighbour pairs Al–Al are avoided, the intensities of the lines appearing in the ^{29}Si NMR spectra of A-type zeolites can be related to the second-neighbour correlation S_2. The fractions of Al–Al, Al–Si and Si–Si atom pairs in second-neighbour T sites are given by

$$\begin{aligned} Z_{Al-Al} &= x_{Si}(\tfrac{1}{6}C_2 + \tfrac{1}{2}C_3 + C_4) \\ Z_{Al-Si} &= x_{Si}(\tfrac{1}{2}C_1 + \tfrac{2}{3}C_2 + \tfrac{1}{2}C_3) \\ Z_{Si-Si} &= x_{Al} + x_{Si}(C_0 + \tfrac{1}{2}C_1 + \tfrac{1}{6}C_2) \end{aligned} \tag{9}$$

where C_n are the concentrations of the Si environments displayed in figure 2. From equation (4), one has

$$S_2 = Z_{\mathrm{Al\text{-}Al}} + Z_{\mathrm{Si\text{-}Si}} - Z_{\mathrm{Al\text{-}Si}} \tag{10}$$

and finally one obtains

$$S_2 = x_{\mathrm{Al}} + x_{\mathrm{Si}}(C_0 + \tfrac{1}{3}C_2 + C_4). \tag{11}$$

Values of S_2 derived by using equation (11) from ^{29}Si NMR spectra of A-type zeolites are presented in figure 4, where filled circles correspond to the specimens analysed by Jarman *et al* [10] and open circles to those studied by Bennett *et al* [9]. In this figure, the full curve is obtained from our MC simulations for interaction model B, whereas the dashed line corresponds to model A (only nearest-neighbour interactions). The agreement between the S_2 values associated with model B and those derived from the NMR data is good in the composition range $65 < n < 96$. For low Al loading ($n < 60$), the agreement is poorer, which can be a consequence of the lack of thermodynamic stability of the synthetic specimens with these compositions, as discussed elsewhere [21, 10]. Model A (only Al–Al avoidance) predicts second-neighbour correlations higher than those found for the real material, in the whole composition range $48 < n < 96$, with the exception of the high-Al-loading region ($x_{\mathrm{Al}}/x_{\mathrm{Si}} \to 1$), where a long-range-order scheme with Si and Al atoms alternating in the netwok is found for both potential models (sub-lattice ordering).

Another feature differentiating the atom ordering corresponding to models A and B is shown in figure 5, where the dependence of the order parameter L on the Al content is compared. As noted above, sub-lattice ordering is found for $x_{\mathrm{Al}} \to 0.5$, independent of the potential model employed in the simulations. For low Al content, the mean atom occupancies of sub-lattices T_a and T_b are equal, and the average $\langle L\rangle_{\mathrm{MC}}$ of the order parameter L over an MC trajectory is zero. The transition from short-range ($\langle L\rangle_{\mathrm{MC}} = 0$) to long-range ordering ($\langle L\rangle_{\mathrm{MC}} \simeq \pm 1$) occurs for the potential model B at about 84 Al atoms per cell ($x_{\mathrm{Al}} = 0.44$), whereas it happens at $n \simeq 68$ ($x_{\mathrm{Al}} \simeq 0.35$) for model A. This indicates that the consideration of long-range Coulomb and polarization energies has an important influence on the sub-lattice ordering in this framework, especially in the region $n = 68$–84, where the $\langle L\rangle_{\mathrm{MC}}$ values found for models A and B are clearly different.

For a given framework composition, the distribution $P(L)$ of L values found from the MC simulations gives information additional to that obtained from the mean value $\langle L\rangle_{\mathrm{MC}}$. The $P(L)$ distribution corresponding to the interaction model B is plotted in figure 6 for several framework compositions, and for $L > 0$. Note that $P(L)$ is an even function of L ($P(L) = P(-L)$) due to the symmetry between the two sub-lattices T_a and T_b. For low Al contents ($n < 70$), the distribution $P(L)$ has nearly a Gaussian form centred at $L = 0$, as can be seen for $n = 48$ in figure 6. In connection to this, a Gaussian $P(L)$ distribution is expected for a random atom arrangement, as discussed below. For $n > 74$, the maximum of $P(L)$ is displaced from $L = 0$, indicating the appearance of ordered domains in the tetrahedral framework, in which the Al atoms occupy mainly one of the two sub-lattices T_a or T_b. The maxima of $P(L)$ are located at the limit values $L = 1$ and -1 for $n > 84$. For framework compositions in the range $82 < n < 92$, one finds a peak of $P(L)$ at $L \simeq 0.9$ from the MC simulations corresponding to model B. As the Al mole fraction increases, this cusp moves slightly to higher L-values, and is absent for $x_{\mathrm{Al}} \simeq 0.5$. Following the definition of L (equation (5)), this peak will be associated with a definite number of antisites, which will be favoured by the geometry of the network and the interaction potential. The shoulder at $L \simeq 0.8$ (indicated by an arrow in figure 6) is reproducible for compositions of about 84 Al atoms per simulation cell.

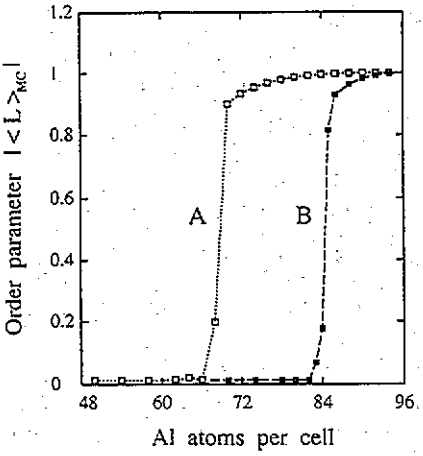

Figure 5. Absolute value of the averaged order parameter $\langle L\rangle_{MC}$ for model A (open squares) and B (filled squares) as a function of the Al loading.

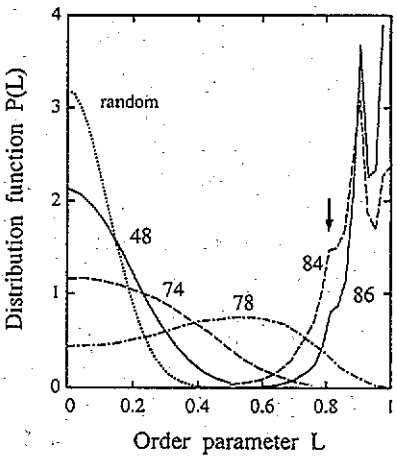

Figure 6. Distribution functions $P(L)$ of the order parameter L found from MC simulations for potential B corresponding to several framework compositions. Labels indicate the number of Al atoms per simulation cell. The dotted curve was obtained for a random atom arrangement from equation (18). The area under the curves is normalized to unity. An arrow indicates a shoulder appearing in the $P(L)$ curves for $n \simeq 84$.

4. Discussion

From the results obtained for the second-neighbour pair correlation S_2 presented in figure 4, it is clear that consideration of atom interactions further than nearest-neighbour tetrahedra is necessary to understand the ^{29}Si NMR data. This could be expected if one takes into account that Si and Al atoms will feel long-range interactions in the zeolitic frameworks. The fact that S_2 in the actual material is lower than that found for only the avoidance of Al atoms in contiguous tetrahedra indicates that atoms of the same type (Si or Al) repel each other to decrease the concentrations of Al–Al and Si–Si pairs in next-nearest tetrahedra. This contrasts with the affirmations of several authors, in the sense that only the exclusion of Al atoms in nearest T-sites could explain the ^{29}Si NMR spectra of zeolites [31, 32].

The order parameter L presented in figure 5 for our models A and B undergoes a fast increase from $L = 0$ to $|L| \simeq 1$, in agreement with a transition from short- to long-range order in the atom distribution. Note that we have presented $|\langle L\rangle_{MC}|$ instead of $\langle L\rangle_{MC}$, which can take the values ~ 1 or -1 in the long-range order region, according to whether the Al atoms are essentially located on sub-lattice T_a or T_b. However, the average value of L over the whole configuration space, $\langle L\rangle_{can}$, obtained as

$$\langle L\rangle_{can} = \frac{1}{R}\sum_{L} LP(L) \tag{12}$$

where $R = \sum_L P(L)$, is zero for all framework compositions due to the symmetry of the distribution function $P(L)$. The subscript 'can' means that this average corresponds to the canonical ensemble. This indicates that, in the MC simulations for high n, the system becomes 'frozen' in one of the two regions of the configuration space corresponding to the two energy minima of the system. Of course, in different MC runs, one can explore these

two different parts of the configuration space. Following Palmer [33], we will assign a component (a or b) to each one of these configuration regions.

For the MC simulations for which $\langle L\rangle_{MC} = \pm 1$, the system remains confined in one component (say a) and cannot pass to the other (b) in the finite time of a simulation run. However, due to the finite size of our simulation cell, one expects that the change from one ground state to the other should be obtained in a finite number n_0 of MC steps. The results concerning the order parameter L for $n_S = 5 \times 10^5$ MC steps are reproducible, and we guess that values of n_0 much higher than this number are necessary to invert the Si and Al sub-lattices, especially for x_{Al} values near 0.5. An indication that our cell size and n_S value are adequate to study the atom ordering in zeolite A is given by a similar MC simulation of the Si, Al distribution in faujasite-like zeolites [17]. For the latter, an x-ray diffraction study found a discontinuity of the lattice parameter as a function of the Al loading at $x_{Al} = 0.42$ [34]. The MC simulations carried out at the formation temperature of faujasites found a change from short- to long-range order at the same value of x_{Al}. Unfortunately, for A-type zeolites there are no available x-ray data for the x_{Al} dependence of the lattice parameter, and a direct comparison with our order parameter L is not possible.

Information on the atom ordering, complementary to that found from the average order parameter $\langle L\rangle_{MC}$, can be obtained from the mean square fluctuations of L along an MC run. These fluctuations are defined as

$$(\Delta L)^2_{MC} = \langle L^2\rangle_{MC} - \langle L\rangle^2_{MC}. \tag{13}$$

For the canonical ensemble, one has $\langle L\rangle_{can} = 0$, and then

$$(\Delta L)^2_{can} = \langle L^2\rangle_{can}. \tag{14}$$

Values of $(\Delta L)_{MC}$ obtained from the MC simulations at temperature T_F for the interaction models A and B are shown in figure 7 (white and black symbols). For comparison, we present also the RMS fluctuations $(\Delta L)_{can}$, which follow the dotted curves in this figure. For increasing Al loading, $(\Delta L)_{MC}$ grows and then undergoes a sudden decrease at the x_{Al} value where $\langle L\rangle_{MC}$ goes to values typical of long-range ordering ($\sim \pm 1$). The fast decrease in $(\Delta L)_{MC}$ is due to the confinement of the system in one of the two components a or b. For $x_{Al} = 0.5$, $(\Delta L)_{MC} \simeq 0$, since the distribution function $P(L)$ consists approximately of two δ functions at $L = \pm 1$, and $(\Delta L)_{can} = 1$.

Whenever the system is confined in one component (say a), by taking into account that $\langle L\rangle_{can} = 0$, it is straightforward to see that

$$(\Delta L)^2_{can} = (\Delta L)^2_a + \langle L\rangle^2_a \tag{15}$$

where a indicates that the average is performed over that component. When the ergodicity is broken, this equation is fulfilled by the values of $(\Delta L)_{MC}$, $\langle L\rangle_{MC}$ and $(\Delta L)_{can}$ shown in figures 5 and 7, since the averages over the MC trajectories are restricted in each case to one component of the configuration space. When the MC trajectory is not confined to one component ($x_{Al} < 0.35$ for model A, and $x_{Al} < 0.44$ for model B), the canonical prescription gives the same results as the MC simulations, and $(\Delta L)_{can} = (\Delta L)_{MC}$ (see figure 7).

The break of ergodicity observed for x_{Al} near 0.5 is similar to that appearing in magnetic systems with Ising-like interactions, as was discussed extensively by Palmer [33]. In fact, the same trend of $P(L)$ to split into two δ functions, discussed here, is obtained for spin

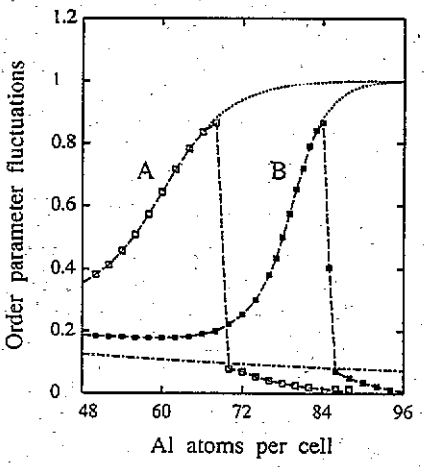

Figure 7. RMS fluctuations of the order parameter L obtained from MC simulations by means of equation (13) for the interaction models A (open squares) and B (filled squares). The dotted curves correspond to $(\Delta L)_{can}$ for the whole canonical ensemble. The chain curve represents the RMS fluctuations $(\Delta L)_R$ obtained for a random atom arrangement by using equation (19).

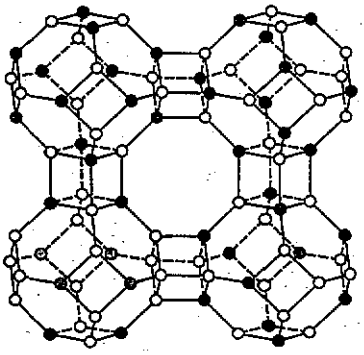

Figure 8. Sketch of the zeolite-A framework showing an Si, Al configuration obtained from MC simulation at 400 K for model B and $n = 84$. Open circles indicate Si atoms; filled and shaded circles represent Al atoms on sites T_a and T_b, respectively.

systems from MC simulations at low temperatures [35]. In our case, the break of ergodicity is associated with a decrease in the symmetry of the material. This means that one has the space group $Fm\bar{3}c$ (two sets T_a and T_b of tetrahedral sites with different atom occupancy) for x_{Al} near 0.5, versus the space group $Pm\bar{3}m$ (only one crystallographic T site) for $x_{Al} < 0.44$.

As indicated above, the distribution of L values, $P(L)$, for $n < 70$ has a nearly Gaussian shape. In order to compare our results with the $P(L)$ distribution expected for a random atom arrangement on a cell with N_T sites, we employ the following approach. We call N_S the number of sites in each sub-lattice per simulation cell ($N_S = N_T/2$). Then the number M_R (R stands for random atom arrangement) of distinguishable microstates with n_1 Al atoms on sub-lattice T_a and n_2 Al atoms on sub-lattice T_b ($n_1 + n_2 = n$), is given by

$$M_R = [N_S!/n_1!(N_S - n_1)!]N_S!/n_2!(N_S - n_2)!. \tag{16}$$

If we call $\Delta n = n_1 - n_2$, by using the Stirling formula for the factorials and Taylor expanding $\log(n + \Delta n)$ up to the second power of $\Delta n/n$, one finds for M_R the Gaussian approximation

$$M_R = M_0 \exp[-Q(\Delta n)^2] \tag{17}$$

where M_0 is the number of microstates with $\Delta n = 0$, and $Q = N_S/[n(2N_S - n)]$. Making use of equations (5) and (7), one has $\Delta n = N_S(x_{Al,1} - x_{Al,2}) = nL$, and then one finds for $P_R(L)$ the Gaussian distribution

$$P_R(L) = P_R(0) \exp(-Qn^2L^2). \tag{18}$$

This distribution is plotted in figure 6 for $n = 48$ (dotted curve), along with those obtained from the MC simulations corresponding to model B. It is clear that even for low Al content

($n = 48$), the $P(L)$ distribution obtained from the MC simulations is broader than that associated with a random atom arrangement. This is a consequence of the non-negligible atom correlations, which propagate through the simulation cell, even in the cases where $\langle L\rangle_{MC} = 0$.

The RMS deviation of the order parameter L for a randon atom distribution is given from equation (18) by

$$(\Delta L)_R = 1/n\sqrt{2Q}. \tag{19}$$

This value of ΔL coincides with the mean square fluctuations of L obtained in MC simulations performed at high temperatures. This should be expected, since in the limit $T \to \infty$, the atom distribution is random. Note that the width of the L distribution depends on the cell size (N_T) and on the mole fraction $x_{Al} = n/N_T$. In the thermodynamic limit $N_T \to \infty$, $(\Delta L)_R$ goes to zero as $N_T^{-1/2}$. The n dependence of $(\Delta L)_R$ is shown in figure 7 (chain curve) for the cell size employed in our MC simulations. For framework compositions for which $\langle L\rangle_{MC} = 0$, $(\Delta L)_{MC}$ is clearly higher than $(\Delta L)_R$, as should be expected from the second-neighbour pair correlations S_2 presented in figure 4. On the other hand, when the MC trajectory is confined to one component (a or b), one finds $(\Delta L)_{MC} < (\Delta L)_R$.

From a structural point of view, the peak of $P(L)$ at $L \simeq 0.9$ appearing for framework compositions with $n = 84$–90 (see figure 6) will be due to some particular disposition of the Al antisites in the Si sub-lattice. From equation (7), the number n_A of Al antisites is given by

$$n_A = \tfrac{1}{2}n(1 - L) \tag{20}$$

which means that, for example, for $n = 84$, the peak at $L = 0.905$ corresponds to $n_A = 4$. This indicates that a group of four antisites is energetically favoured in the range of compositions $n = 84$–90. The peak of $P(L)$ moves slightly to higher L values for increasing n in the region $n = 84$–90 in agreement with a fixed value $n_A = 4$ in equation (20). Such a group of four Al-antisites is shown in the left-hand bottom part of figure 8, where black and white circles represent Al and Si atoms, respectively. The four shaded circles correspond to Al atoms on the Si sub-lattice. The atom distribution displayed in figure 8 was obtained from MC simulation using model B for $n = 84$, but the same disposition of antisites has been found to be favoured for Al contents up to $n = 90$. The shoulder of $P(L)$ at $L \simeq 0.8$ indicated by an arrow in figure 6 corresponds to $n_A = 8$, and is associated with the presence of two groups of Al antisites similar to that shown in figure 8. For the simulation model A, however, no indication of such a cusp in the $P(L)$ distribution is observed, which means that the particular disposition of antisites shown in figure 8 is due to the inclusion of Coulomb interaction and O polarization in our potential model. Note that, although there is no experimental evidence of the presence of these groups of Al antisites in the zeolite-A framework, the second-neighbour pair correlation presented in figure 4 indicates that for framewok compositions with $n \simeq 84$, the S_2 values derived from ^{29}Si NMR spectra agree better with MC simulations for model B than for model A. Thus for model B, the energetic stabilization of this type of antisite grouping will favour a decrease of $|L|$ with respect to model A, contributing to displace the appearance of long-range order to higher x_{Al} concentrations, in agreement with the results shown in figure 5.

5. Conclusions

The interaction potential B, which takes into account the presence of long-range Coulomb interactions and the polarization energy of the O atoms of the framework, gives good

agreement with the short-range order of the tetrahedral atoms in the actual A-type zeolites. The consideration of atom interactions further than nearest tetrahedra is fundamental to find quantitative agreement between ^{29}Si NMR spectra and MC simulations.

Although the order parameter L goes from 0 to 1 in the considered composition range for both potential models A and B, the composition at which sub-lattice ordering appears depends markedly on the potential used in the simulations. The break of ergodicity appearing in the MC simulations for framework compositions near $x_{Al} = 0.5$ is consistent with the existence of two different types of tetrahedral sites T_a and T_b, as observed by x-ray analysis (space group $Fm\bar{3}c$).

Acknowledgments

R Ramirez is thanked for critical comments on the manuscript. This work was supported by CICYT (Spain) under contract MAT91-0394.

References

[1] Jacobs P A and van Santen R A (ed) 1989 *Zeolites: Facts, Figures, Future, Studies in Surface Science and Catalysis* vol 49 (Amsterdam: Elsevier)
[2] Preuss E, Linden G and Peuckert M 1985 *J. Phys. Chem.* **89** 2955
[3] Sauer J 1989 *Chem. Rev.* **89** 199
[4] Shin J M, No K T and Jhon M S 1988 *J. Phys. Chem.* **92** 4533
[5] Song M K, Chon H and Jhon M S 1990 *J. Phys. Chem.* **94** 7671
[6] Demontis P, Suffritti G B, Quartieri S, Fois E S and Gamba A 1988 *J. Phys. Chem.* **92** 867
[7] Melchior M T, Vaughan E W, Jarman R H and Jacobson A J 1982 *Nature* **298** 455
[8] Smith J V and Pluth J J 1981 *Nature* **291** 265
[9] Bennett J M, Blackwell C S and Cox D E 1983 *J. Phys. Chem.* **87** 3783
[10] Jarman R H, Melchior M T and Vaughan D E W 1983 *Am. Chem. Soc. Symp. Ser.* **218** 267
[11] Klinowski J 1984 *Prog. NMR Spectrosc.* **16** 237
[12] Engelhardt G and Michel D 1987 *High Resolution Solid State NMR of Silicates and Zeolites* (New York: Wiley)
[13] Dutta P K and Del Barco B 1988 *J. Phys. Chem.* **92** 354
[14] Vega A J 1983 *Am. Chem. Soc. Symp. Ser.* **218** 217
[15] Soukoulis C M 1984 *J. Phys. Chem.* **88** 4898
[16] Herrero C P 1991 *J. Phys. Chem.* **95** 3282
[17] Herrero C P, Utrera L and Ramirez R 1992 *Phys. Rev.* B **46** 787
[18] Herrero C P, Utrera L and Ramirez R 1991 *Chem. Phys. Lett.* **183** 199
[19] Pluth J J and Smith J V 1980 *J. Am. Chem. Soc.* **102** 4704
[20] Putnis A and Angel R J 1985 *J. Phys. Chem. Minerals* **12** 217
[21] Herrero C P 1993 *J. Phys. Chem.* **97** 3338
[22] Ooms G, van Santen R A, den Ouden C J J, Jackson R A and Catlow C R A 1988 *J. Phys. Chem.* **92** 4462
[23] Catlow C R A 1988 *Physical Properties and Thermodynamic Behaviour of Minerals (NATO Adv. Study Inst. C225)* ed E K H Salje (Dordrecht: Reidel) p 619
[24] Jackson R A 1990 *Computer Modelling of Fluids, Polymers and Solids (NATO Adv. Study Inst. C293)* ed C R A Catlow, S C Parker and M P Allen (Dordrecht: Kluwer) p 395
[25] Herrero C P and Ramirez R 1992 *J. Phys. Chem.* **96** 2246
[26] Metropolis N, Rosenbluth A W, Rosenbluth M N, Teller A H and Teller E 1953 *J. Chem. Phys.* **21** 1087
[27] Binder K and Heermann D W 1988 *Monte Carlo Simulation in Statistical Physics* (Berlin: Springer)
[28] Kirkpatrick S, Gelatt C D Jr and Vecchi M P 1983 *Science* **220** 671
[29] Loewenstein W 1954 *Am. Mineral.* **39** 92
[30] Bell G M and Davies D A 1989 *Statistical Mechanics of Lattice Models* vol 1 (New York: Ellis Horwood)
[31] Beagley B, Dwyer J, Fitch F R, Mann R and Walters J 1984 *J. Phys. Chem.* **88** 1744
[32] Corma A, Fornés V, Melo F V and Herrero J 1987 *Zeolites* **7** 559

[33] Palmer R G 1982 *Adv. Phys.* **31** 669
[34] Dempsey E, Kühl G H and Olson D H 1969 *J. Phys. Chem.* **73** 387
[35] Binder K 1981 *Z. Phys.* B **43** 119